N84 27283

SOME CASE STUDIES OF OCEAN WAVE PHYSICAL PROCESSES UTILIZING THE GSFC AIRBORNE RADAR OCEAN WAVE SPECTROMETER

F. C. Jackson
NASA Goddard Space Flight Center
Laboratory for Atmospheric Sciences
Greenbelt, Maryland, USA

ABSTRACT

The NASA K_u-band Radar Ocean Wave Spectrometer (ROWS) is an experimental prototype of a possible future satellite instrument for low data rate global waves measurements. The ROWS technique. which utilizes short-pulse radar altimeters in a conical scan mode near vertical incidence to map the directional slope spectrum in wave number and azimuth, is briefly described. The potential of the technique is illustrated by some specific case studies of wave physical processes utilizing the aircraft ROWS data. These include i) an evaluation of numerical hindcast model performance in storm sea conditions, ii) a study of fetch-limited wave growth, and iii) a study of the fully-developed sea state. Results of these studies, which are briefly summarized, show how directional wave spectral observations from a mobile platform can contribute enormously to our understanding of wave physical processes.

1. INTRODUCTION

A simple method for measuring the vector wave number spectrum of ocean surface gravity waves from aircraft and satellite platforms using modified radar altimeters has been described and investigated theoretically by Jackson (1981) and demonstrated experimentally by Jackson et al. (1984a). In this paper, rather than dwell on the details of the technique, we will present some specific aircraft results that will serve to illustrate the enormous potential of this measurement technique for furthering our understanding of wave physical processes.

The GSFC K_u-band Radar Ocean Wave Spectrometer (ROWS) is a noncoherent, short pulse radar that uses a near-nadir directed conically scanning antenna to map wave directionality. Table 1 gives the pertinent instrument characteristics. Figure 1 depicts the aircraft measurement geometry. A small rotarty antenna boresighted to 16° incidence produces a footprint at the nominal 10 km aircraft altitude measuring approximately 1500 m in the range (x) dimension and 700 m in the orthogonal azimuthal (y) dimension. The surface is probed in the range dimension using 12.5 ns compressed pulses. At the nominal incidence angle for peak power return, $\theta = 13°$, the surface range resolution is 8 m. The directional resolution of the ROWS is obtained by a simple phase front matching condition between electromagnetic and ocean wave Fourier contrast wave components across the relatively broad azimuth beamwidth. That is, the broad beamwidth functions to isolate, or resolve, ocean Fourier components whose wave vectors $\underline{k} = (k, \phi)$ are aligned with with the radar azimuth ϕ. In this respect, the ROWS technique is similar to the dual frequency technique investigated by Alpers and Hasselmann (1978). Let the fractional cross section variation for any pixel (x, y) be denoted $\delta\sigma/\sigma$. The fractional reflectivity modulation m seen by the radar is given by $\delta\sigma/\sigma$ averaged laterally across the beam. If G(y) denotes the lateral gain pattern, then

RADAR OCEAN WAVE SPECTROMETER

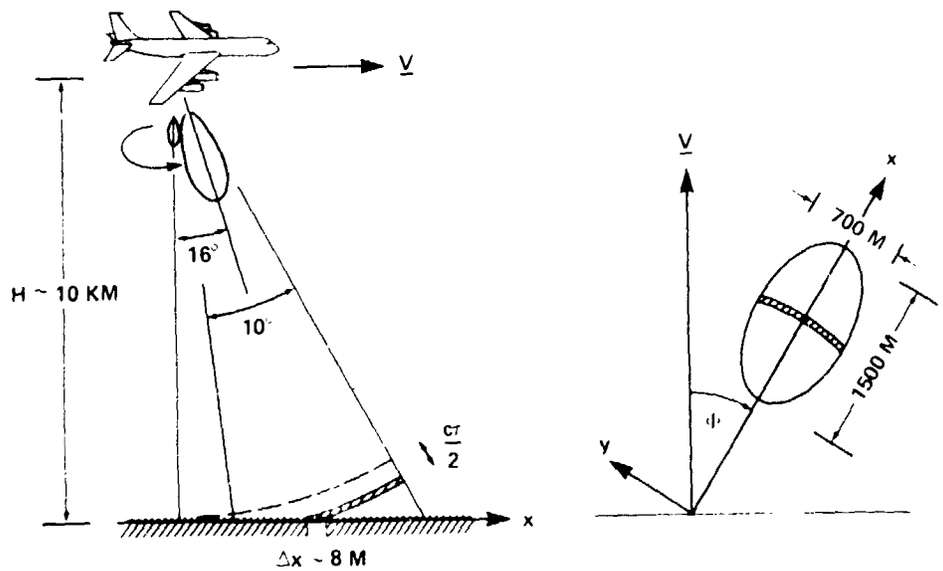

Figure 1. ROWS Measurement Geometry.

TABLE 1. ROWS INSTRUMENT CHARACTERISTICS

Frequency:	13.9 GHz
Pulse type:	Linear FM, 100 MHz, 1.2 μs chirp
Pulse length:	12.5 ns compressed
Peak power:	2 kW
PRF:	100 Hz max
Detection:	Noncoherent, square law
Antenna:	10° elevation X 4° azimuth printed circuit, 16° incidence boresight, 6 rpm rotation rate
Data:	Digital, max 1024 six bit word frame size, sample gate width selectable 2, 5, ... ns; recording at full PRF

$$m(x, \phi) = \delta W/W = \frac{\int G^2(y)(\delta\sigma/\sigma)dy}{\int G^2(y)dy} \qquad (1)$$

where $\delta W/W$ is the fractional modulation in received power (averaged over the clutter fluctuations).

In the near-vertical specular backscatter regime in which the ROWS operates, the cross-section variation is primarily a geometrical tilting effect, hydrodynamic modulation effects being of second order. Provided the large-wave steepness is small compared to the total surface roughness as measured by the total (diffraction-effective) mean square slope β^2, then the cross section variation will be proportional to the large-wave slope component in the plane of incidence $\partial\zeta/\partial x$ as

$$\frac{\delta\sigma}{\sigma} = \left(\cot\theta - \frac{1}{\sigma^\circ}\frac{\partial\sigma^\circ}{\partial\theta}\right)\frac{\partial\zeta}{\partial x} \qquad (2)$$

where θ is the angle of incidence and σ° is the average cross section of the surface. In (2) the first term represents a linearized area tilt term while the second term represents the rigid rotation of the small-scale scattered power pattern by the large wave slopes. The average cross section is proportional to the probability density function of surface wave slopes evaluated at the specular condition for backscatter (namely, slope = tan θ). Assuming a Gaussian isotropic distribution of slopes, the cross-section roll-off is given approximately by

$$\frac{1}{\sigma^\circ}\frac{\partial\sigma^\circ}{\partial\theta} = -\frac{2\tan\theta}{\beta^2} \tag{3}$$

where again β^2 is the total mean square slope.

Assuming that the water wavelength $2\pi/k$ is small compared to the azimuth beamwidth L_y, $kL_y \gg 1$, it follows that the spectrum of $m(x, \phi)$ is proportional to the directional wave slope spectrum. If the gain pattern is assumed to be Gaussian, $G(y) = \exp(-y^2/2L_y^2)$, one finds that in the limit of large kL_y the directional modulation spectrum is given by

$$P_m(k, \phi) = \frac{\sqrt{2\pi}}{L_y}\left[\cot\theta - \frac{2\tan\theta}{\beta^2}\right]^2 k^2 F(k, \phi) \tag{4}$$

where F is the polar-symmetric directional height spectrum, defined such that the height variance,

$$\langle r^2\rangle = \int_0^\infty\int_0^\pi F(k, \phi)\,k\,dk\,d\phi \tag{5}$$

We note that in (1) the azimuth coordinate y was treated as rectilinear; this is permissible for directionally spread seas. The wave front curvature enters, along with the finite footprint size and antenna rotation, in determining the directional resolution. In the satellite case the resolution is typically 7° (200 m water wave), while in the aircraft case the resolution is typically 20°.

The ROWS data processing, described in detail in Jackson et al. (1984a), consists of first correcting for the wave front sphericity on a pulse by pulse basis on going from the signal delay time to the surface range coordinate x, and then integrating the pulse returns in surface-fixed range bins over a time corresponding to 15° of antenna rotation (N = 42 pulses). The surface tracking is accomplished using an input aircraft speed. The modulation $m(x, \phi)$ is then computed by normalizing by an estimate of the average power envelope $\langle W(x, \phi\rangle$ obtained by averaging over several antenna rotations. Unity is then subtracted and the data are rewindowed and the spectrum $P_m(k, \phi)$ computed by fast Fourier transform. The final estimates of P_m are obtained by averaging the spectra over several antenna rotations, subtracting a computed residual fading spectrum, and correcting for the finite pulse response (20% spectral roll-off at 40 m wavelength).

We note that the tilt model solution (4) has been shown by Jackson (1981) to correspond to the first term in a series expansion of the geometrical optics solution for P_m, where the ordering parameter is the large-wave steepness. Nonlinear terms, both electromagnetic and hydrodynamic, were found to be small provided that i) β^2 is sufficiently large (wind speeds greater than ca. 5 ms^{-1}), ii) the incidence angle lies in the range of 8°-16°, and iii) the large-wave slope is not too large (steepness < 0.10). The ROWS technique in general, and the tilt model result in particular, have been extensively validated by Jackson et al. (1984a). In the following, we will illustrate the power of the ROWS technique

by presenting several case studies of ocean wave physical processes utilizing the ROWS data. The data to be shown have been transformed from slope spectra to height spectra in the frequency domain assuming the linear deep-water dispersion relationship. Also, we have symmetrized the observed 360° modulation spectrum so that it is strictly polar-symmetric (this has the effect of doubling the degrees of freedom and eliminating any upwave/downwave asymmetry that may result from second order effects). The height spectra are computed from the symmetrized modulation spectra according to

$$S(f, \theta) = (2/\alpha f)\, P_m(k, \theta) \qquad (5)$$

where α is the sensitivity coefficient, the factor of k/F in (4), f is the frequency in Hz, and where S is defined so that the variance $\langle \eta^2 \rangle = \int\int S(f, \theta)\, df\, d\theta$. The final spectra shown here were obtained from nine or ten beam rotations, and so the degrees of freedom of the directional spectral estimates shown here number no less than 2 × 2 × 9 = 36. The degrees of freedom for the nondirectional spectra number several hundred (these confidence limits are not shown).

2. EVALUATION OF HINDCAST MODEL PERFORMANCE IN STORM CONDITIONS

Our present understanding of the basic physics of ocean waves is to a large extent embodied in numerical wave forecast/hindcast models, specifically, in the right hand side of the spectral energy transport equation. Considerable uncertainty exists in the parameterization of wave spectral growth (and decay) under the action of variable winds, particularly in the specification of directional distributions and the redistribution of wave energy over direction in turning wind fields. This is abundantly clear from Hasselmann's (1984) model intercomparison report. We have undertaken a study with V. Cardone (Oceanweather, Inc.) comparing ROWS data taken in the Norwegian Sea during an intense storm to special hindcast runs with well-specified wind fields (or as well-specified as possible). The comparison is particularly interesting because the storm not only produced very high seas (ca. 10 m), but created a complex, rapidly evolving wave field. The comparison thus provides a strong test of model performance. Initial model runs have been made with a fine-mesh (100 km/3 hr) version of Cardone et al.'s (1976) ODGP discrete spectral model (a variant of the U. S. Navy's operational SOWM model) and with a coupled discrete model, the SAIL model (cf. Hasselmann, 1984). The hindcasts used all available ship wind reports on record and aircraft winds obtained during a low-level flight leg. The modeled area was the N. E. Atlantic, and the spin up time (before the flight of interest) was two weeks.

The NASA Ames' CV-990 flight track and ROWS data takes between ca. 0800 Z and 1000 Z on Nov. 3, 1978 are shown in Figure 2 along with the nearby ODGP model grid points. The flight track constitutes a box pattern measuring ca. 150 km (N-S dimension) by 700 km (SW-NE direction). The aircraft altitude was ca. 10 km. Ten ROWS files were obtained in the flight box; these are indicated by the letters A-J in Figure 2. At the northern end of the box, close to file A, is the weather station Tromsoflaket (TROMSO) which provided 3-hourly wind reports and Waverider wave spectra observations. The synoptic situation at 1800 Z on Nov. 2 at about the peak of the storm is shown in Figure 3. By flight time, the low had moved to the north of the box, and the winds had shifted to westerly over the northern end of the box. The high pressure ridge also moved northward, its axis transecting the midsection of the box at the time of the flight. Figure 4 is a presentation of the ten files of ROWS data in the form of polar contour plots of directional height spectra laid out on a map of the Norwegian Sea. The spectra, contoured at equal intervals, are scaled to the peak values; absolute

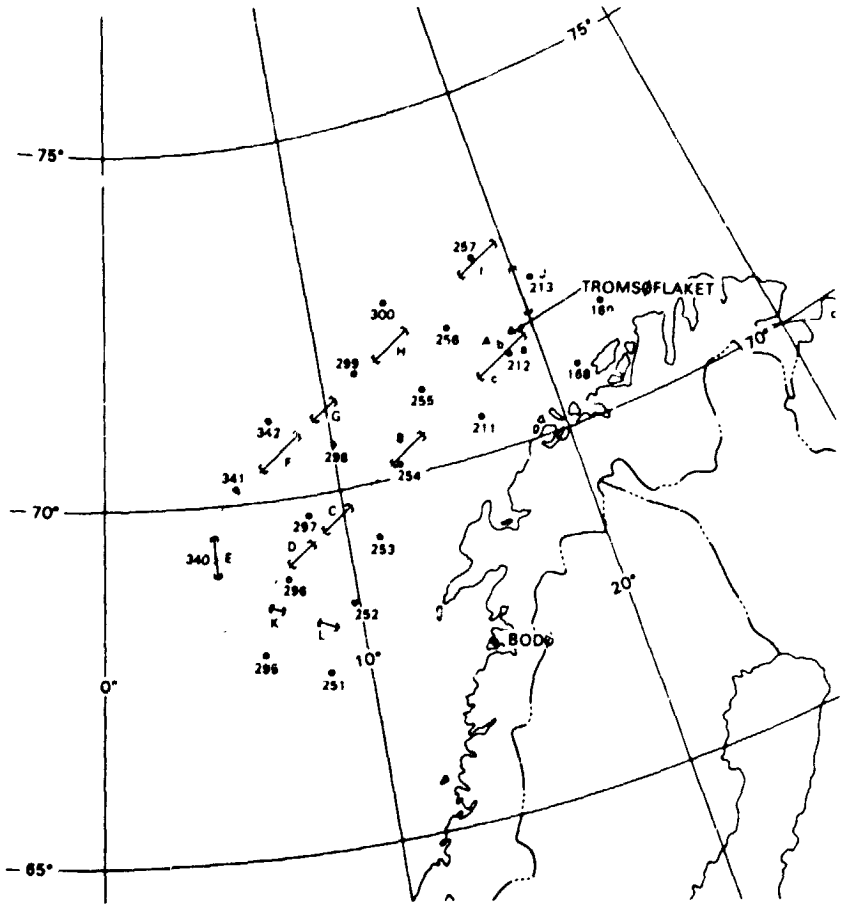

Figure 2. CV-990 Flight Track and ROWS Data Takes on Nov. 3, 1978, 0800-1000 Z.

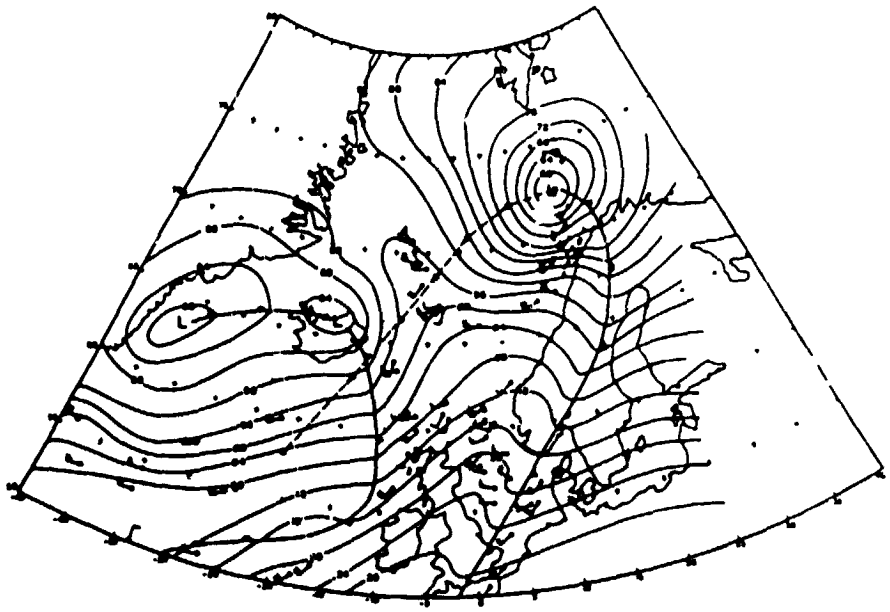

Figure 3. Nov. 2 1800 Z Synoptic Chart Showing Norwegian Sea Storm.

energy levels are indicated by the estimated significant wave heights given numerically in meters beside each spectrum. The spectra shown are one-sided. The 180° ambiguity in the ROWS spectra was resolved and the true direction of wave travel determined on the basis of the synoptic situation. The synoptic view of the wave field in Figure 4 shows two major wave trains traveling at nearly right angles to each other. The NE travelling component appears to enter the box at the southern end more or less as swell, decay slightly, and then grow rapidly in the stronger winds in the northern end of the box, where the winds are westerly at ca. 20 ms^{-1}. The NE direction of this wave train is maintained over the entire 700 km distance of the flight legs. Only at the northernmost location does one see energy appearing in the local wind direction (this is evident in the comma shape of file A). The SE traveling component is evidently a pulse of wave energy generated in the western sector of the rapidly moving cyclone at about the 1800 Z map time (Figure 3).

Figure 1. ROWS Directional Height Spectra in Norwegian Sea Storm. Tic marks are 0.05 Hz. Spectra are scaled to peak values. The numbers indicate wave heights in meters.

An indication of the quality of the ROWS data is given by Figure 5, which compares the nondirectional spectrum of file A/subfile a with the TROMSO Waverider spectrum. The agreement is seen to be excellent.

The results of the first ODGP model run showed basically good agreement with the ROWS and TROMSO significant wave heights and nondirectional spectra. However, comparison of directional spectra showed immediately that the model had failed to produce the SE travelling component in the strength observed. This was seen to be due a poor kinematic analysis for the data-sparse western sector of the cyclone. Figure 6 compares the ROWS spectrum for file b with the ODGP hindcast spectrum for grid point 254 (0900 Z) in FNOC/SOWM/ODGP variance format. Only a trace of the SE travelling component is seen at higher frequency. We see further in Figure 6 that the hindcast is also severely underestimating the strength of the NE travelling component, which is only weakly represented in the hindcast as an islet of energy near 0.065 Hz. The hindcast is evidently putting the energy of the NE component (to 45°) into the local wind direction (to 90°). While the model errors here are obvious, it is important to note that they are often masked in the nondirectional spectrum: Thus, the nondirectional spectra corresponding to Figure 6 shown in Figure 7 are quite close and give no clue as to the seriousness of the actual hindcast error. That the model should perform better for the integrated properties should not be surprising since the greatest uncertainty in wave models today lies in the modelling of the directional response to varying winds (the directional relaxation problem).

A second ODGP model run with a new kinematic analysis of the western sector of the cyclone essentially correctly reproduced the observed SE directed components. However, the model still tended to place more energy in the local wind direction than actually observed. A first run of the SAIL model exaggerated this tendency in the ODGP. Additional runs with the SAIL model will be made with slower directional relaxation rates; also the the nondirectional growth rates will be tuned to maximize the agreement with the ROWS (and TROMSO) wave observations. In summary, this hindcast comparison shows i) how the ROWS observations pointed immediately to wind field specification errors, and ii) that the directional relaxation rates, especially of the newer-generation coupled models (cf., Hasselmann, 1984) are too fast. This latter observation is supported by the results of the next case study.

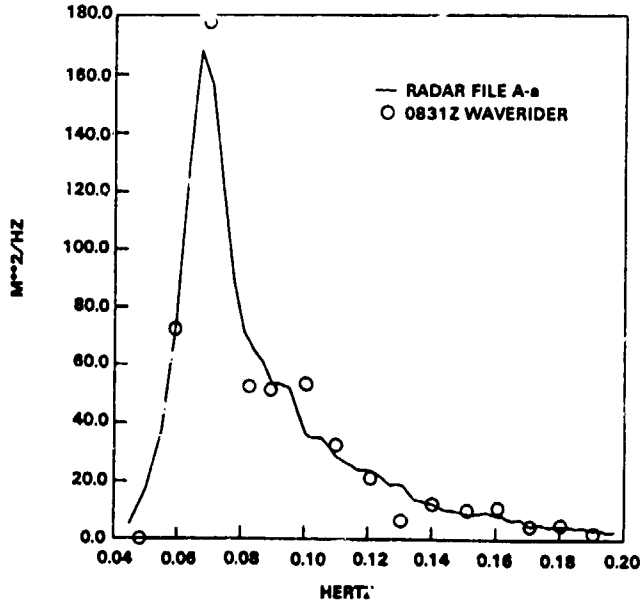

Figure 5. Comparison of ROWS Nondirectional Spectrum with TROMSO Waverider.

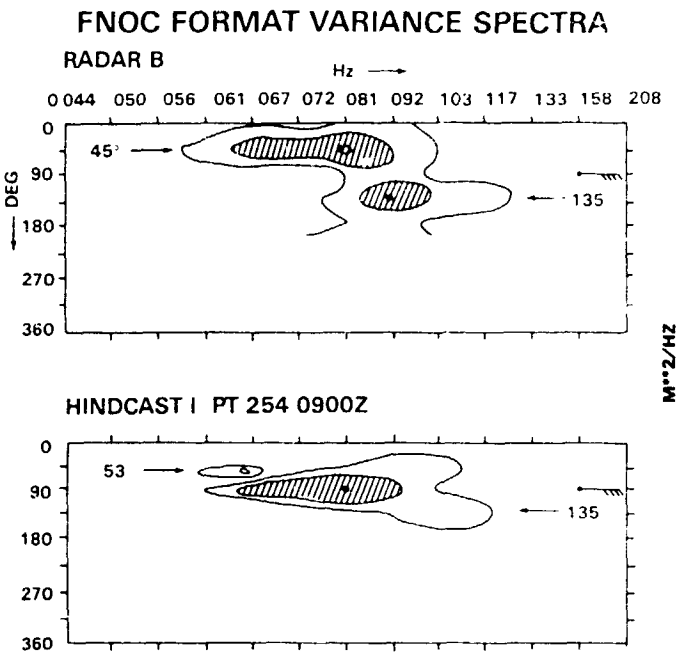

Figure 6.

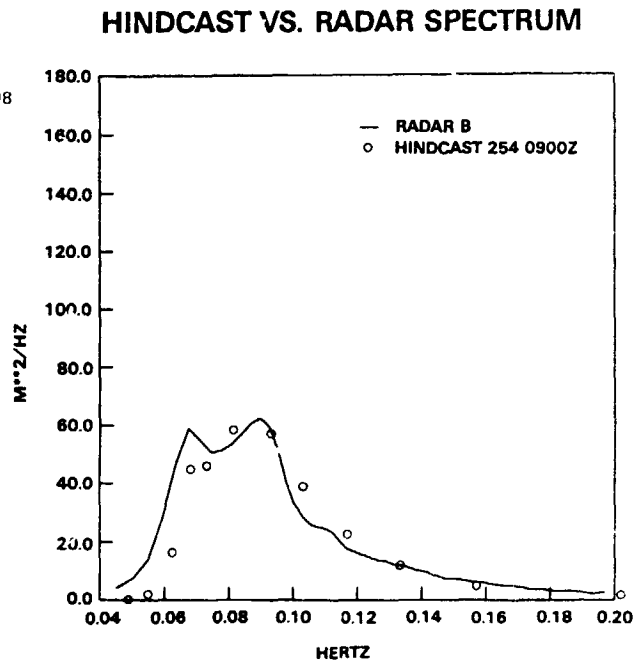

Figure 7.

3. FETCH LIMITED WAVE GROWTH OBSERVED DURING MASEX

The GSFC radar was installed on the NASA Wallops' P-3 aircraft in 1982 with an improved antenna system installation (which eliminated diffraction problems experienced in the Fall '78 Mission data). The main reason for the switch of platforms for the ROWS was to be able to fly in concert with E. Walsh's Surface Contour Radar (SCR), a 36 GHz, direct topographic mapping radar, in order to obtain high resolution directional spectra for intercomparison/validation purposes. The ROWS participated in three joint flights with the SCR during the MASEX (Mesoscale Air-Sea Exchange) experiment in January 1983. Besides systems intercomparison, the flight objective was to obtain data on the evolution of the directional spectrum with fetch during strong cold air outbreaks off the east coast of the U. S. Figure 8 shows the ROWS flight track (7 km altitude) for the 1/16 MASEX flight, the tape/file numbers being indicated by numbers and letters. The wind was approximately 12 ms^{-1} blowing offshore normal to the coast and to within a few degrees of the flight track. Figure 9 is a selection of the ROWS directional height spectra from the 1/16 flight. Figure 10 shows the entire sequence of ROWS-inferred nondirectional spectra for the flight leg extending out to ca. 300 km. The ROWS directional spectra of Figure 9 show two nearly equally energetic wave components, one travelling downwind, the other travelling in directions nearly opposite to the line-of-sight directions to the mouth of the Delaware Bay. The angles of the 'Delaware Bay' component are seen to be steeper than the line-of-sight angles to the mouth of the bay; this is apparently due to refraction near the mouth of the Bay. The existence of this strong off-wind component was first discovered by Walsh et. al. (1982). It is evidently due to fact that the waves outside the mouth of the bay have a 'leg up' over the waves further south along the coast. These waves may then enter a more rapid growth stage (Miles' growth) earlier than the downwind waves along the track. There is also the possibility that these waves are preferentially grown (in file 4-c these waves are

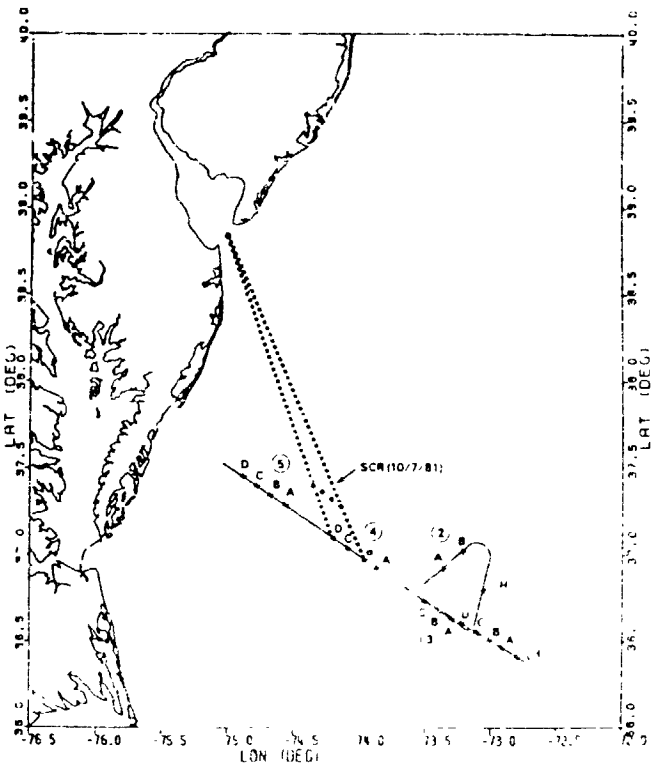

Figure 8. Flight Track and ROWS Data Takes for MASEX 1/16/83 Flight. Wind is normal to coast and parallel to flight track.

seen to exceed the downwind component) because they are very close to the Phillips' resonance curve (shown as the horizontal line in Figure 9). Most im-important, we observe in these spectra that over the entire fetch the off-wind component does not turn into the wind direction: It is not 'absorbed' by the 'local wind sea' (downwind component) until its mean direction lies well within the directional spread of the downwind component. This observation runs counter to current theory (Hasselmann, 1984) which would ascribe a strong directional coupling to the two components. On the contrary, the two components appear to be uncoupled, or at the most only weakly coupled. This behavior is consistent with what we have observed in the Norwegian Sea hindcast study. Preexisting components are not easily turned into the wind direction, nor do they tend to be absorbed by the local wind sea. This conclusion was reached also by Holthuijsen (1983) who found strong off-wind components in fetch-limited spectra in the North Sea, also due to coastline irregularities. The ROWS (and SCR) spectra from the two other MASEX flights similarly show strong off-wind components that point clearly to major embayments in the Middle Atlantic Bight. Similarly, also, these components appear to be decoupled from the downwind component. Figure 11 is a ROWS height spectrum from a flight down-fetch of Long Island which shows dominant wave energy not in the wind direction (to 160°), but at an angle pointing to the center of the Block Island/Rhode Island Sound complex.

The ROWS data of Figure 11 can be compared to nearly colocated SCR data in Figure 12. The overall agreement is seen to be excellent. Slight discrepancies are most likely due colocation discrepancies, both spatial and temporal. It is worth noting here that apart from stereo photography, only the SCR could have provided this kind of high resolution intercomparison data.

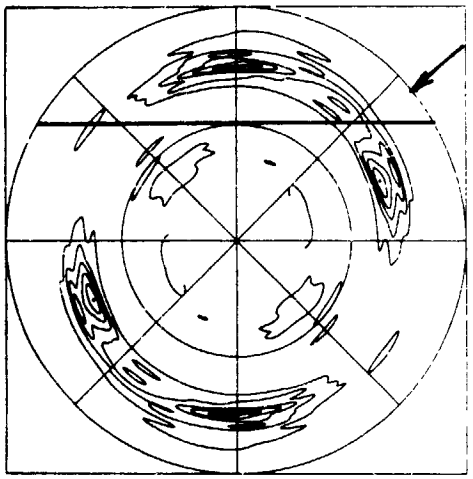

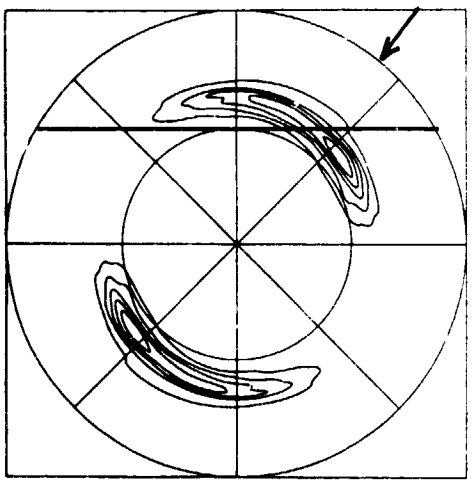

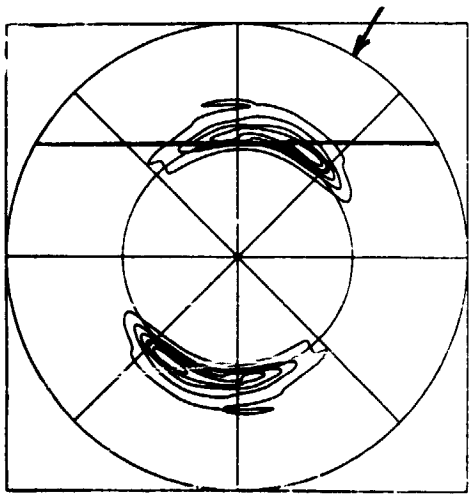

Figure 9. Examples of ROWS Directional Height Spectra from 1/[illegible]33 MASEX Flight. From top to bot[illegible]he files shown are (cf. Figure 8, 5B, 4C, and 3C. The aircraft heading, equals the (anti) wind direction, is to the top of the page. The arrows indicate the line-of-sight angles to the mouth of the Delaware Bay. The horizontal lines are the Phillips' resonance curve. The spectra are contoured with six equally spaced contour intervals scaled to the peak values. Frequency rings are 0.10 Hz and 0.20 Hz.

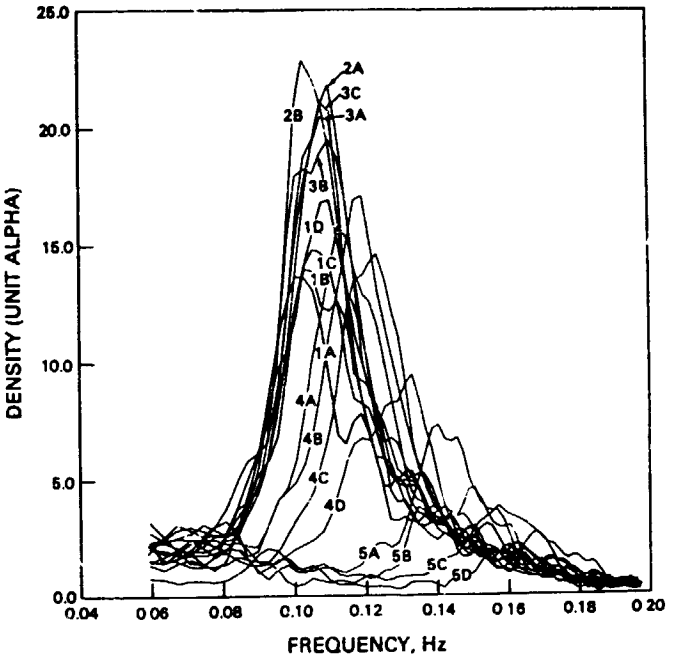

Figure 10. ROWS Nondirectional Spectra from 1/16 MASEX Flight for Unit Sensitivity Coefficient.

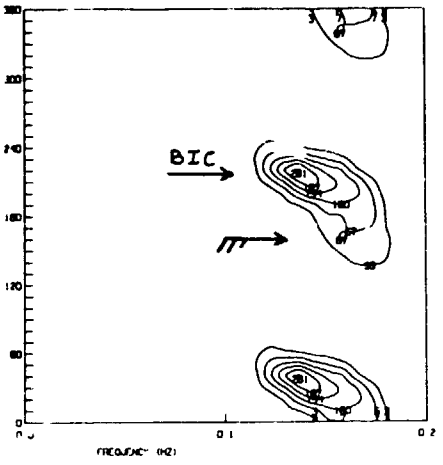

Figure 11. ROWS Height Spectrum from 1/20 MASEX Flight. BIC is Block Island Component.

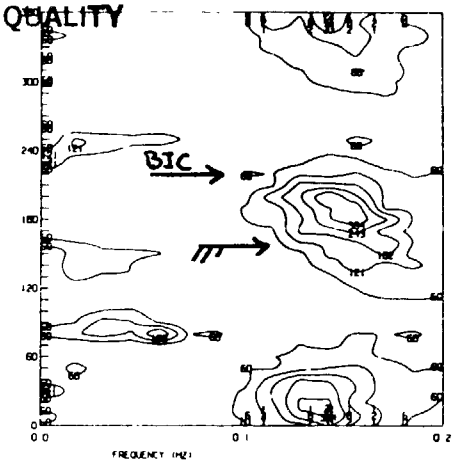

Figure 12. SCR Height Spectrum for Comparison to Figure 11. Colocation is not exact.

A thorough analysis of the MASEX data set should go a long way to resolving some fundamental issues in the physics of wind-generated ocean waves, at least in the macroscopic, or practical modelling sense.

4. 'THE SON OF SWOP'-- AN OBSERVATION OF A FULLY DEVELOPED SEA

A detailed analysis of a Fall '78 Mission ROWS observation of a fully developed sea in the N. E. Pacific and intercomparison with a pitch-roll buoy is given by Jackson (1984b). The ROWS-observed directional spectrum of the 3.3 m significant wave height sea is given in Figure 13, and the nondirectional comparison with the buoy is given in Figure 14. The directional comparison (not shown here) gave excellent agreement in terms of the mean wave directions and directional spreads as functions of frequency.

The observed spectrum in Figure 13 bears such a remarkable resemblance to the classical SWOP (Stereo Wave Observation Project) spectrum (Pierson, 1960) that we have dubbed this ROWS spectrum 'The Son of SWOP'. The two spectra have nearly identical half power widths (80° at peak to 120° at high frequency), and both spectra exhibit nearly identical bimodal structures which accord with the Phillips' resonance condition. The Phillips' resonance angles γ , determined according to the resonance condition,

$$U_c \cos \gamma = c(f) = g/2\pi f \qquad (6)$$

where U_c is the windspeed, or convection velocity, and c is the water wave phase speed, are indicated by the arrows in Figure 15, where $U_c = 14.2$ ms^{-1} is chosen to give $\gamma = 0$ at $f = 0.11$ Hz. The agreement with the observed modal angles is seen to be very good. This observation is seen to confirm Phillips' original contention (Phillips, 1958) that the SWOP spectrum bimodality was a real manifestation of the resonance mechanism and not a statistical fluke.

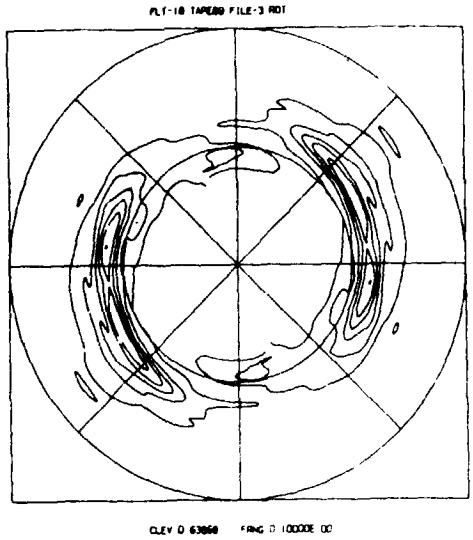

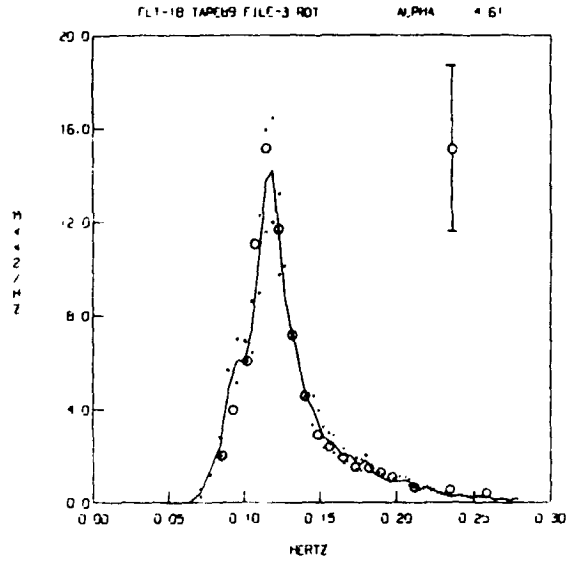

Figure 13. 'Son of SWOP' Height Spectrum. Contouring as in Figure 9.

Figure 14. Nondirectional Height Spectrum Corresponding to Figure 13. Solid line is radar, circles buoy. Dots are radar confidence intervals.

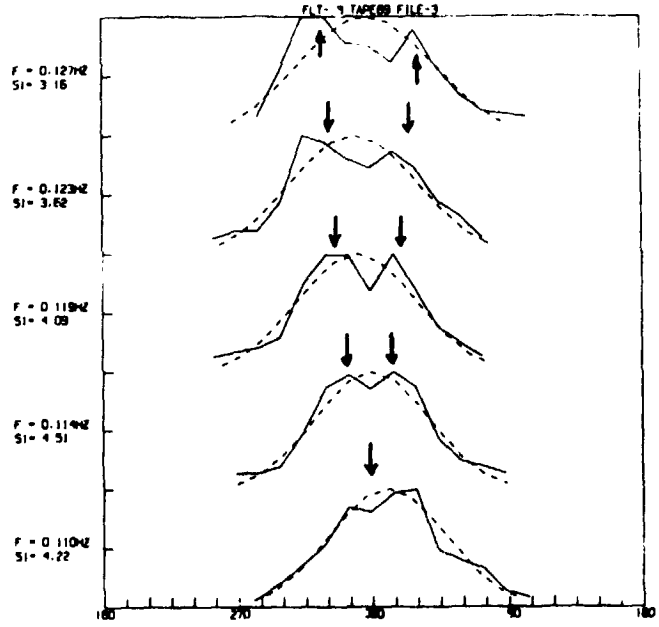

Figure 15. 'Son of SWOP' Directional Cuts (Normalized to Peak) with Philips' Resonance angles indicated by arrows.

5. CONCLUSION

This paper has emphasized the use of the ROWS in case studies of wave physical processes. The results, while preliminary, give an idea of the enormous potential of this remote sensing technique. Further study of the Norwegian Sea case and the MASEX data shoud permit more concrete, quantitative statements regarding wave growth and directional relaxation. The 'Son of SWOP' observation fairly conclusively demonstrates that the Philips' resonance mechanism is indeed operative in the the fully developed sea state and is a major factor in determining the directional structure.

We have not dwelt on the details of the ROWS technique here, its accuracy, or its ultimate space application. These aspects have been extensively delt with in Jackson (1981) and Jackson et al. (1984a). However, the reader may appreciate the remarkable accuracy of the indirect ROWS measurements by again examining the Waverider buoy, SCR, and pitch-roll buoy comparisons given respectively in Figures 5, 12, and 14: The technique appears to be very accurate, at least for sea states above 1 m, and providing the windspeed is greater than ca. 5 ms^{-1}. Similar accuracy is possible with a spacecraft system employing present generation short pulse radar altimeters.

6. REFERENCES

Alpers, W. and K. Hasselmann, 1978: The two-frequency microwave technique for Measuring ocean wave spectra from an airplane or satellite. Boundary-Layer Meteorol., 13, 215-230.

Cardone, V., W. J. Pierson, and E. G. Ward, 1976: Hindcasting the directional directional spectrum of hurricane-generated waves. J. Petrol. Technol., 385-394.

Hasselmann, K. (Ed.), 1984: Sea Wave Modeling Project. Proc. Symp. Wave Dynamics and Radio Probing of the Ocean Surface, Plenum Press (in press).

Holthuijsen, L. H., 1983: Observations of the directional distribution of ocean wave energy in fetch-limited conditions. J. Phys. Oceanog., 13, 191-207.

Jackson, F. C., 1981: An analysis of short pulse and dual frequency radar techniques for measuring ocean wave spectra from satellites. Radio Sci., 16, 1385-1400.

Jackson, F. C., W. T. Walton, and P. L. Baker, 1984a: Aircraft and satellite measurement of ocean wave directional spectra using scanning-beam microwave radars. Proc. Symp. Wave Dynamics and Radio Probing of the Ocean Surface, Plenum Press (in press).

Jackson, F. C., W. T. Walton, and C. Y. Peng, 1984b: A comparison of in-situ and airborne radar observations of ocean wave directionality. J. Geophys. Res. (in press).

Phillips, O. M., 1958: On some properties of the spectrum of wind-generated ocean waves. J. Marine Res., 16, 231-240.

Pierson, W. J. (Ed.), 1960: The directional spectrum of a wind-generated sea as determined from data obtained by the Stereo Wave Observation Project. Meteorol. Papers, 2, (6), New York Univ., New York.

Walsh, E. J., D. W. Hancock, III, D. E. Hines, and J. E. Kenney, 1982: Development of the fetch-limited directional wave spectrum. Oceans '82 Conference Record, Marine Tech. Soc., Wash., D. C., 820-825.